Journal of Catalysis 337 (2016) 208–220

Contents lists available at ScienceDirect

Journal of Catalysis

journal homepage: www.elsevier.com/locate/jcat

Understanding the generation of methanol synthesis and water gas shift activity over copper-based catalysts – A spatially resolved experimental kinetic study using steady and non-steady state operation under $CO/CO_2/H_2$ feeds

S.K. Wilkinson [a,b,*], L.G.A. van de Water [a], B. Miller [c], M.J.H. Simmons [b], E.H. Stitt [a], M.J. Watson [a]

[a] Johnson Matthey Technology Centre, Billingham, PO Box 1, TS23 1LB, UK
[b] School of Chemical Engineering, University of Birmingham, Birmingham B15 2TT, UK
[c] Jembec Consulting, 18 Country Palms Drive, Christchurch 8025, New Zealand

ARTICLE INFO

Article history:
Received 27 November 2015
Revised 21 January 2016
Accepted 22 January 2016
Available online 27 February 2016

Keywords:
Methanol synthesis
Water gas shift
Active site
Micro kinetics
Steady state
Transient

ABSTRACT

Understanding the mechanism and generation of activity for methanol synthesis and the water gas shift reactions over copper-based catalysts remains a significant area of study in heterogeneous catalysis. In this work, steady and non-steady state experimental and kinetic modelling methods are presented to demonstrate changes in functionality of a $Cu/ZnO/Al_2O_3$ catalyst based on gas composition.

Steady-state testing of a $Cu/ZnO/Al_2O_3$ catalyst, using experimental spatial discretisation approaches with fixed-bed, integral-operation micro reactors, has generated performance data over a range of P_{CO}/P_{CO2} ratios (1–10). The data showed a mixture of observations where forward or reverse water gas shift was kinetically favourable, and also where the reaction was significantly limited by thermodynamic equilibrium. A steady state Langmuir–Hinshelwood model based on micro kinetics was most appropriate which includes kinetic descriptions of both directions of the water gas shift reaction. Using this method, the entire dataset could be predicted and an internal consistency within the kinetic model of the key adsorption constants was demonstrated.

Non-steady state, 'reactor start-up', testing of a $Cu/ZnO/Al_2O_3$ catalyst marked a novel approach to further understanding the functionality of the catalyst. Initial changes in surface carbon and oxygen populations were quantified and linked to subsequent dynamic changes in methanol synthesis and water gas shift activity. Cu/ZnO and Cu/Al_2O_3 formulations were also evaluated and tested using kinetic models, permitting a structural and compositional comparison with $Cu/ZnO/Al_2O_3$.

1. Introduction

Methanol (CH_3OH) has a long history as a key industrial chemical, chiefly serving as an intermediate in the production of other chemicals such as formaldehyde and methyl-tert-butyl ether (MTBE). Methanol has also recently found increased use in alternative fuel applications such as fuel cells [1]. The world production of methanol was ~62 million metric tonnes in 2014,[1] a figure which is increasing annually. The industrial production of methanol via catalytic technologies has been carried out for over 90 years, following the original commercialisation of a process by BASF in 1923. Since then, the production of methanol has seen significant developments on a practical level (in terms of catalyst and process improvements) but also on a scientific level, to understand the fundamentals of how this catalytic process actually works.

The catalytic synthesis of methanol from mixtures of $CO/CO_2/H_2$ (termed 'syngas') was the second major industrial application of catalysis, following that of ammonia synthesis [2]. Unlike ammonia synthesis however, it is critical to deliver a catalyst that is both *active* and *selective* to the methanol synthesis reaction as unwanted reactions may occur. Under $CO/CO_2/H_2$ conditions the following catalytic reactions may be prevalent:

$$CO_2 + 3H_2 \Longleftrightarrow CH_3OH + H_2O \quad (\Delta H_{298} = -41.17\ \text{kJ mol}^{-1}) \tag{1}$$

$$CO_2 + H_2 \Longleftrightarrow CO + H_2O \quad (\Delta H_{298} = +49.47\ \text{kJ mol}^{-1}) \tag{2}$$

$$CO + 2H_2 \Longleftrightarrow CH_3OH \quad (\Delta H_{298} = -90.64\ \text{kJ mol}^{-1}) \tag{3}$$

* Corresponding author at: Johnson Matthey Technology Centre, Billingham, PO Box 1, TS23 1LB, UK.
E-mail address: sam.wilkinson@matthey.com (S.K. Wilkinson).
[1] *Source:* IHS Chemical.

http://dx.doi.org/10.1016/j.jcat.2016.01.025
0021-9517/

Nomenclature

a_i	power dependency on methanol synthesis rate expression (–)
A	pre-exponential factor (s^{-1} (for 1st order))
b_i	power dependency on reverse water gas shift rate expression (–)
$B(t)$	sensitivity function (–)
CC	parameter cross correlation matrix (–)
d_p	particle size diameter (μm)
E_a	activation energy (kJ mol^{-1})
F	F-value (–)
k	rate constant (s^{-1} (for 1st order))
K	adsorption equilibrium constant (bar^{-1} (for 1st order))
K^*	thermodynamic constant (–)
P	partial pressure (bar)
Par	number of parameters (–)
r	rate of reaction (mol m^{-3} s^{-1} (for intrinsic rates unless noted))
R	universal gas constant (J K^{-1} mol^{-1})
s	active site (–)
t	time (s)
T	temperature (K)
v_m	molar volume (m^3)
y	model response (–)
Z	compressibility factor (–)

Greek letters

β^*	thermodynamic equilibrium value (–)
ΔH_{ads}	heat of adsorption (kJ mol^{-1})
ΔH_{298K}	heat of reaction (kJ mol^{-1})
κ_{CC}	condition number (–)

Subscripts

base	of base temperature
i	of species
melting	melting point

Acronym

FWGS	forward water gas shift
IR	infrared
MFC	mass flow controller
RWGS	reverse water gas shift
STP	standard temperature and pressure

Eqs. (1) and (3) describe methanol synthesis via hydrogenation of CO_2 and CO respectively and are both mildly exothermic. Eq. (2) is the reverse water gas shift (RWGS) reaction and is mildly endothermic. The industry standard catalyst for this process is a $Cu/ZnO/Al_2O_3$ formulation which was developed by ICI in the 1960s. This catalyst formulation enabled higher activity than its ZnO/Cr_2O_3 predecessor whilst operating at much lower pressures and temperatures (<100 bar, <573 K), therefore increasing plant efficiency and greatly reducing operating costs.

The methanol synthesis process over a $Cu/ZnO/Al_2O_3$ catalyst has attracted great research interest and debate over the past 40 years. Central to this has been the pursuit of the nature of the active site(s) for the methanol synthesis and RWGS reactions and also the reaction mechanisms by which these reactions proceed. Early kinetic studies for this system assumed that CO was the source of carbon in the synthesis of methanol [3]. Subsequent works [4,5] noticed discrepancies in catalyst performance based on the CO_2 content of the syngas feeds, leading to a maximum in the methanol production rate over integral operation reactors at P_{CO}/P_{CO2} ratios of 5–10. The key argument placed at the time was that CO_2 could help maintain a degree of oxidised copper sites on the catalyst surface.

The works of Liu and co-workers, Chinchen and co-workers [6,7] greatly altered the views on the reaction pathway for methanol synthesis over $Cu/ZnO/Al_2O_3$ catalysts. In the former, an isotope labelling study using ^{18}O CO_2 found that the source of carbon in methanol under $CO/CO_2/H_2$ conditions was in fact CO_2 not CO. In the latter, a linear trend between copper metal surface areas and CO_2 hydrogenation activity of a wide range of copper-based formulations was found. Linked to this, CO_2 partial pressure has a linear relationship with methanol production rate under differential conditions [8].

From this link of copper metal surface area with CO_2 hydrogenation pathway as the critical step in determining methanol synthesis activity, the rest of this introduction will examine kinetics and mechanistic developments. The main focus will be to identify gaps in understanding of the linkage between catalyst formulation, functionality and feed content under reaction conditions.

1.1. Kinetic modelling of copper-based catalysts in the literature under $CO/CO_2/H_2$ conditions

Table 1 shows a selection of key kinetic models proposed in the literature based on operation under $CO/CO_2/H_2$ conditions. The model of Mochalin and co-workers [9] was unique at the time of writing as it completely disregarded the CO hydrogenation to methanol route, owing to the fact the authors were never able to synthesise methanol over a $Cu/ZnO/Al_2O_3$ catalyst under CO/H_2 conditions. Water inhibition is apparent in both the methanol synthesis (from CO_2) and RWGS routes described but the work expanded no further on this or the physical basis of the overall model. Similar models have been proposed subsequently [10,11].

The model of Graaf and co-workers [12] was proposed based on a statistical discrimination approach whereby experimental data from a spinning basket reactor were fitted to 48 different kinetic models. A similar model more recently was also proposed by Lim and co-workers [13]. The concerns with the final model lie in its physical basis, which does not acknowledge that certain surface intermediates can feature in more than one overall reaction [14]. Instead all reactions are assumed to proceed via individual routes.

In the work of Graaf and co-workers [12] the magnitude of the estimated value of $\Delta H_{ads,CO}$ is close to a number of estimations in the literature for the adsorption of CO on a Cu^0 surface which are in the range of 42–53 kJ mol^{-1} [15,16]. CO coverage under methanol synthesis conditions was shown to be low in these works, however, which brings the significance of this parameter into question. The value is also similar to the reaction of CO with surface oxygen on a $Cu/ZnO/Al_2O_3$ surface to form $CO_2(ads)^-$ in the range of 64–80 kJ mol^{-1} [17,18]. Many works support a redox mechanism for the WGS reaction, of which the formation of $CO_2(ads)^-$ occurs in the forward direction [14,19]. It is therefore plausible that r_3 in this network is a lumped descriptor of forward water gas shift (FWGS) and CO_2 hydrogenation to methanol activity, rather than a separate mechanistic route for methanol synthesis from adsorbed CO. This may also explain the error in the fitted RWGS pre-exponential factor if the reaction network is over-determined.

The work of Coteron and Hayhurst [20] refuted the existence of a CO hydrogenation route under $CO/CO_2/H_2$ conditions and instead

Table 1
Selected kinetic models for methanol synthesis under $CO/CO_2/H_2$ conditions taken from the literature.

Model	Rate expressions: $r_1 = CO_2 \rightarrow CH_3OH$ $r_2 = CO_2 \rightarrow CO$ $r_3 = CO \rightarrow CH_3OH$	Exp. conditions tested	Fitted activation energies or heat of adsorption (kJ mol^{-1})
Mochalin et al. [9] (Eq. (4))	$r_1 = \frac{k_1 P_{CO_2} P_{H_2} \left(1 - K_1^* \left(P_{MeOH} P_{H_2O} / \left(P_{CO_2} P_{H_2}^3\right)\right)\right)}{\left(P_{CO_2} + K' P_{CO_2} P_{H_2O} + K'' P_{H_2O}\right)}$ $r_2 = \frac{k_2 P_{CO_2} P_{H_2} \left(1 - K_2^* \left(P_{CO} P_{H_2O} / \left(P_{CO_2} P_{H_2}\right)\right)\right)}{\left(P_{CO_2} + K' P_{CO_2} P_{H_2O} + K'' P_{H_2O}\right)}$	>0% CO_2	Not quoted
Graaf et al. [12] (Eq. (5))	$r_1 = \frac{k_1 K_{CO_2} \left(P_{CO_2} P_{H_2}^{3/2} - P_{MeOH} P_{H_2O} K_1^* / P_{H_2}^{3/2}\right)}{\left(1 + K_{CO} P_{CO} + K_{CO_2} P_{CO_2}\right)\left(P_{H_2}^{1/2} + \frac{K_{H_2O} P_{H_2O}}{K_{H_2}^{1/2}}\right)}$	15–50 bar	$E_{a,1}$ = 65.2
	$r_2 = \frac{k_2 K_{CO_2} \left(P_{CO_2} P_{H_2} - P_{CO} P_{H_2O} K_2^*\right)}{\left(1 + K_{CO} P_{CO} + K_{CO_2} P_{CO_2}\right)\left(P_{H_2}^{1/2} + \frac{K_{H_2O} P_{H_2O}}{K_{H_2}^{1/2}}\right)}$	483–518 K	$E_{a,2}$ = 123.4
	$r_3 = \frac{k_3 K_{CO} \left(P_{CO} P_{H_2}^{3/2} - P_{MeOH} K_3^* / P_{H_2}^{1/2}\right)}{\left(1 + K_{CO} P_{CO} + K_{CO_2} P_{CO_2}\right)\left(P_{H_2}^{1/2} + \frac{K_{H_2O} P_{H_2O}}{K_{H_2}^{1/2}}\right)}$	0–22% CO	$E_{a,3}$ = 109.9
		2–26% CO_2 in H_2 Spinning basket reactor	$\Delta H_{ads,CO2} = -67.4$ $\Delta H_{ads,CO} = -58.1$ $\Delta H_{ads,H2O/H2} = -104.5$
Coteron and Hayhurst [20] (Eq. (6))	$r_1 = \frac{k_1 K_{CO_2} K_{H_2} K_{HCO_2}}{1 + K_{CO_2} P_{CO_2} + K_{CO} K_{H_2}^{1/2} K_{HCO_2} P_{CO_2} P_{H_2}^{1/2} + \frac{K_{CO_2} P_{CO_2}}{K_{CO} P_{CO}}}$	10 bar 473–523 K 10–20% CO 10–20% CO_2 in H_2 Differential operation	$E_{a,1}$ = 47.0 $\Delta H_{ads,CO2} = 0$ $\Delta H_{ads,H2} = -6.3$
Vanden Bussche and Froment [14] (Eq. (7))	$r_1 = \frac{k'_{MeOH} P_{CO_2} P_{H_2} \left(1 - K_1^* \left(P_{MeOH} P_{H_2O} / \left(P_{CO_2} P_{H_2}^3\right)\right)\right)}{\left(1 + K_{redox} \frac{P_{H_2O}}{P_{H_2}} + \sqrt{K_{H_2} P_{H_2}} + K_{H_2O} P_{H_2O} + K_{CO_3} P_{CO_2} \sqrt{P_{H_2}} + K_{HCO_2} \frac{P_{CO_2} P_{H_2O}}{P_{H_2}}\right)^3}$	15–51 bar	$E'_{a,MeOH} = -36.7$
	$r_2 = \frac{k_2 P_{CO_2} \left(1 - K_2^* \left(P_{CO} P_{H_2O} / \left(P_{CO_2} P_{H_2}\right)\right)\right)}{\left(1 + K_{redox} \frac{P_{H_2O}}{P_{H_2}} + \sqrt{K_{H_2} P_{H_2}} + K_{H_2O} P_{H_2O} + K_{CO_3} P_{CO_2} \sqrt{P_{H_2}} + K_{HCO_2} \frac{P_{CO_2} P_{H_2O}}{P_{H_2}}\right)}$		$E_{a,2}$ = 94.8
		453–553 K P_{CO}/P_{CO2} = 0–4.1 Integral operation	$\Delta H_{ads,H2} = -17.2$ $\Delta H_{ads,H2O} = -124.1$

left the role of CO purely to the removal of oxygen from the catalyst surface. The authors did not include a thermodynamic driving force term or WGS kinetics into their model.

The model of Vanden Bussche and Froment [14] is a mechanistically driven steady state model for methanol synthesis and WGS reaction under $CO/CO_2/H_2$ conditions. The active site for both reactions was assumed to occur over the copper component of the catalyst, which was assumed to be partially oxidised and contain surface oxygen, denoted O.s. The hydrogenation of surface formate (HCO_2.2s) was assumed to be the rate determining step for methanol synthesis from CO_2 based on previous temperature programmed desorption (TPD) studies [21,22]. The RWGS reaction, proceeding via a redox mechanism, is rate-determined by the dissociative adsorption of CO_2. The model considers all possible surface intermediates in the reaction network. The final model in this work found the populations of surface carbonates and formates to be insignificant and the adsorption constants K_{CO3} and K_{HCO2} were discounted. However for investigations of new Cu-based formulations, or under conditions outside of the scope of this work it would be prudent to include them from the start of a kinetic investigation.

Other kinetic studies under $CO/CO_2/H_2$ conditions in the literature which link with catalyst formulation include the micro-kinetic models from Topsøe [16]. In these works, the authors place great emphasis on oxygen vacancies at Zn–O–Cu interfaces, the proportion of which are believed to change as a function of the redox potential of the syngas (ratio of 'reducing' CO and H_2 gas to 'oxidising' CO_2 and H_2O). A change in the number of oxygen vacancies (Zn-[ ]-Cu) has been shown to impact on copper surface morphology and particle surface area, directly impacting methanol synthesis activity. They suggest that methanol synthesis from CO_2 is therefore a structure sensitive reaction. The opposite is suggested by Chinchen and Spencer [23] who state that Cu surface area is critical to methanol synthesis activity but other parameters such as shape and size distribution of metal crystallites are not.

A recent work by Peter and co-workers [24] examined power law, Langmuir–Hinshelwood (LH) [14] and dynamic micro-kinetic [16,25] models using experimental data under $CO/CO_2/H_2$ conditions and found all levels of model to be very similar in their predictions. This could suggest that the dynamic nuances of the micro-kinetic models based on feed composition may not be critical to predict accurately the methanol synthesis performance of $Cu/ZnO/Al_2O_3$ formulations under $CO/CO_2/H_2$. The extent of conditions for which this is true would require further scrutiny.

1.2. Aims and objectives

From an examination of the literature to date, there are a number of kinetic studies which investigate the mechanisms behind the methanol synthesis reaction under $CO/CO_2/H_2$. Whilst there is considerable agreement on the mechanism of CO_2 hydrogenation to methanol over copper-based catalysts, there is still scope to increase understanding around the generation of catalytic activity under these conditions. This is particularly true at high P_{CO} to P_{CO2} ratios where large shifts are seen in differential and integral methanol productivity.

Additionally, few studies exist in the literature which analyse the reactor start-up (both H_2/N_2 reduction step and onset of $CO/CO_2/H_2$ conditions) at realistic pressures in an experimental rig. In the light of this, the aims for this study are as follows:

Table 2
Compositional and structural data of catalyst precursor formulations used in this study.[a]

Catalyst precursor	Precursor composition (weight %)	BET surface area before reduction step ($m^2\ g^{-1}$)	Cu surface area before reduction step ($m^2\ g^{-1}$)	Cu surface area following reduction step ($m^2\ g^{-1}$)
$CuO/ZnO/Al_2O_3$	60/30/10	97.9	32.4	41.1
CuO/ZnO	34/66	31.8	16.0	17.1
CuO/Al_2O_3	25/75	205.1	6.4	7.4

[a] Data supplied by C. Ranson and R. Fletcher (both of Johnson Matthey).

- Demonstrate how spatially discretised experimental methods can be used to probe steady and non-steady state behaviour of copper-based catalyst formulations under integral reactor operation.
- Develop mechanistically sound steady state kinetic models to describe behaviour of a model ternary $Cu/ZnO/Al_2O_3$ catalyst under $CO/CO_2/H_2$ conditions. This will address P_{CO}/P_{CO2} ratios of 1–10 where significant changes in methanol production rate for integral reactors are observed.
- Analyse non-steady state behaviour of a $Cu/ZnO/Al_2O_3$ catalyst during initial exposure to $CO/CO_2/H_2$ conditions to understand physical and/or chemical transformations which the catalyst may undergo during this period of operation and link this to generation/loss of active sites for methanol synthesis.
- Apply models to experimental performance data of binary catalyst formulations (Cu/ZnO and Cu/Al_2O_3). Compare observations with the ternary catalyst formulation and link catalyst functionality, formulation and impact of feed gas.

2. Materials and methods

2.1. Sample preparation and properties

Three catalysts were chosen for this study, which were all tested in pellet form (particle size range $180 < d_p < 355$ μm). Key structural details of the respective precursor formulations are described in Table 2. The catalyst prior to the reduction step is in its fully oxidic form ($CuO/ZnO/Al_2O_3$). The reduction step in question is described in Table 4.

Copper surface areas were measured using reactive frontal chromatography [26]. This technique is based on the decomposition of nitrous oxide (N_2O) molecules over a reduced copper surface yielding chemisorbed oxygen atoms and nitrogen (N_2), the latter of which is released into the gas phase:

$$N_2O_{(g)} + 2\,Cu_{(s)} \rightarrow N_{2(g)} + (Cu{-}O{-}Cu)_{(s)} \quad (8)$$

In this equation *s* denotes a surface atom. The copper surface areas supplied were measured at 333 K. In these conditions it has been shown that oxidation of metallic copper by N_2O is mild and only oxidises surface copper atoms to a Cu^+ state, denoted by $(Cu–O–Cu)_{(s)}$ [27]. This test was carried out on the Cu-based formulations in Table 2 following a standard H_2 reduction step discussed in Section 3.1. Following the H_2 reduction step, the Cu in the catalyst formulations was approximated to be completely reduced to Cu^0, based on calculation of oxygen evolved from the sample during reduction.

2.2. Micro-reactor test rig

Reaction studies using the catalyst precursor formulations described in Section 2.1 were carried out in fixed-bed, downflow, steel micro-reactors. Six parallel tubes were used with inner diameter of 3 mm and length of ~20 cm. The use of a $180 < d_p < 355$ μm powder sieve fraction ensured a reactor internal diameter (d_r) to d_p ratio of at least 10 in order to minimise wall effects [28] and prevent large pressure drops [29].

During operation, thermocouples were placed in the jacket walls of all micro-reactors, 10 cm below the reactor inlet. Throughout the experimental program, wall temperature variation between the tubes never exceeded ±1 K and deviation from the oven set point never exceeded ±2 K. The micro-reactors were themselves housed in a nitrogen-purged oven.

Table 3
List of properties of catalyst and experimental setup conditions.

Experimental property	Value			
Catalyst mass (g)	0.125–0.5			
Catalyst and SiC diluent particle size (μm)	180–355			
Reactor diameter (mm)	3			
Temperature range (K)	453–493			
Operating pressure range (bar)	10–35			
Flow rate ($L\ h^{-1}$) (STP)	7.5			
Feed-stocks used (vol.%)	CO	CO_2	H_2	N_2
	0	0	2	98
	3	0.3	67	29.7
	3	1	67	29
	3	3	67	27

Experiments were performed in the absence of heat and mass transport limitations allowing for the measurement of intrinsic rates. Full details of reactor setup and catalyst properties are shown in Table 3. This was confirmed by use of key calculations set out in the literature [30], including calculation of intraparticle mass transport limitations (Wheeler–Weisz Modulus), Mears' criterion for intraparticle heat transport limitations and radial temperature gradients.

To illustrate, transport limitations were calculated *a priori* at the extreme of the test programme operation, namely a 500 mg $Cu/ZnO/Al_2O_3$ catalyst bed operating at 493 K, 35 bar under a 3% CO/3% CO_2/67% H_2/27% N_2 gas mix at steady state. The apparent methanol formation rate was 0.95 μmol g cat^{-1} s^{-1} over this integral bed. Under these conditions, the radial heat transport gradient was 0.01 K, and both internal and external mass transfer efficiencies were >99%. These values satisfy threshold criteria.

In Table 3, CO_x containing gases contain $CO:CO_2$ ratios between 10 and 1. The explored total pressure range is lower than typical industrial operation of ~50 bar; this owed to limitations of the pressure relief valves on the rig. The temperature range of 453–493 K was deliberately chosen so that the catalyst could be operated under conditions that keep catalyst deactivation through sintering to a minimum (such a phenomenon is not directly under investigation in this study).

An assessment can be made using the Hüttig and Tammann approximations, which estimate temperatures for which atoms and bulk phase respectively of the material under consideration become mobile [31]:

$$T > T_{\text{Huttig}} = 0.3T_{\text{melting}} \quad (9)$$

$$T > T_{\text{Tammann}} = 0.5T_{\text{melting}} \quad (10)$$

Cu^0, ZnO and Al_2O_3 have melting points of 1358, 2250 and 2350 K respectively. At the operational extreme (493 K), ZnO and Al_2O_3 are below $T_{\text{Hüttig}}$ at 0.22 and 0.21 (T_{melting}) respectively whilst Cu^0 is above at 0.36 (T_{melting}). To further predict catalyst thermal stability, sintering models for $Cu/ZnO/Al_2O_3$ catalysts were applied over the temperature range [32,33], as well as those examining the

impact of hydrothermal effects [34]. Application of these models revealed that activity loss from sintering over the maximum 50 h of operation in this would be at most 5% of the starting activity. In Section 3.2.1, the stability of the catalyst during testing was checked by consistently returning the catalyst to reference conditions ($CO/CO_2/H_2$: 3/3/67, 473 K, 25 bar).

Parallel difference testing, a methodology demonstrated previously [35,36] was utilised in both steady and non-steady state experiments in this study. The simple setup (see Fig. 1) comprises four tubes in parallel containing 0.125, 0.25, 0.375 and 0.5 g of catalyst respectively. Flow rate (7.5 L h^{-1}), inlet reactant concentration and temperature are the same for each tube throughout the test. Subtraction between the exit concentrations of each catalyst bed at discrete times on stream allows performance to be broken down into four sectors of equal length down the bed. Experimental repeats were carried out as a check for reproducibility. Parallel difference tests were carried out for up to 50 h on stream during the experimental program.

As seen in Fig. 1, each reactor was packed, firstly with SiC ($180 < d_p < 355$ μm), then catalyst (up to 0.5 g), then the remainder with SiC. This ensured that pressure drops, although negligible, were constant across all reactor tubes. The remaining two parallel micro-reactor tubes remained empty during testing and served two purposes:

- To quantify 'blank' activity and show that no homogeneous reaction had occurred.
- To act as a catalyst bed 'bypass' route when new gas feeds were introduced into the experimental rig. This enabled the new gas feeds to fully equilibrate at their true concentration, prior to the individual reactor mass flow controllers, before being fed over the catalysts under testing.

Gases were fed to each micro-reactor tube using 6 PID mass flow controllers (MFCs); one for each reactor. The maximum set point for each MFC was 7.5 L h^{-1} (standard temperature and pressure, STP). The true flow through each MFC relative to respective set point was measured using a rotary gas meter, positioned downstream of the reactors. A 5-point calibration was obtained for all 6 MFCs and was applied to the computer software controlling the rig.

A 6-port valve was positioned downstream of the micro-reactors. Gases from the selected reactor tube were diverted at this valve to an infrared (IR) analyser. Volume % values of CO, CO_2, CH_3OH and H_2O in the reactor effluent were all measured. The IR analyser was calibrated periodically during the experimental program using 6% CO/9.2% CO_2/67% H_2/Balance N_2 (for CO and CO_2 response) and propylene (for CH_3OH and H_2O). The IR analyser provided real time measurements with outputs on a second timescale.

A carbon and oxygen balance was calculated across all reactors at all stages of experimental testing. In this study, carbon and oxygen balances were calculated between 99% and 101% under all steady state tests in this study. Balances under non-steady state conditions are discussed in Section 3.2.3. Measurement and population balance of hydrogen is the only omission in the analysis. Later sections of this study focus on surface population dynamics of carbon and oxygen species, which act as indicators for reaction intermediates and spectator species.

All non-steady state behaviour experiments in this study were triggered by a change in feed conditions over the catalyst beds. These were nominally a switch from 2% H_2/N_2 to $CO/CO_2/H_2$ feeds. A detailed set of blank measurements were carried out for these changes in feed conditions, including:

- Checking all 6 reactors individually.
- Checking the effect of reactor packing.

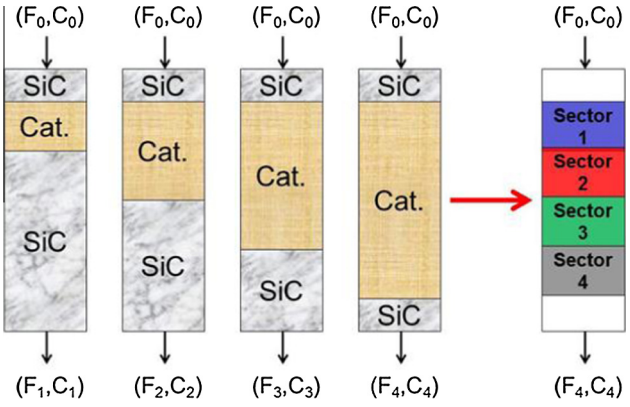

Fig. 1. Parallel difference setup for testing catalysts in this study.

- Examining the effect of temperature and pressure on the measured feed break-through profile.

A study of the above ensured carbon and oxygen could be fully tracked for non-steady state operation during catalyst reaction testing. Relevant blank feed change profiles will be included in the results presentation in Section 3.2.3.

2.3. Kinetic modelling

Parameter estimation within the kinetic models was carried out using Athena Visual Studio© software.[2] The kinetic models tested within this work contain non-linear parameters (e.g. activation energies in the Arrhenius equation) and also include multiple concentration responses. To handle these challenges, two estimation methods were used in succession, namely, *non-linear least squares* and *Bayesian estimation*.

In general, the non-linear least squares method was used for initial discrimination of each of the kinetic models. The objective function of this method is the total residual sum of squares for the entire model. Subsequently the Bayesian estimation method was used to fine tune the parameter estimation outputs. This method considers the error covariance matrix between responses and aligns the objective function accordingly. By this method, any prejudice towards the smaller magnitude responses in the dataset is largely eliminated, enabling a sounder basis for multi-response estimation and a stronger critique of model performance [37]:

$$\frac{dy}{dt} = f(y, Par) \tag{11}$$

In Eq. (11), y denotes model responses, t denotes time and Par denotes the model parameters. A direct decoupled method is used to estimate parametric sensitivities [38]:

$$B(t) = \frac{\partial y(t)}{\partial Par} \tag{12}$$

$$\frac{\partial}{\partial Par}\left(\frac{dy}{dt}\right) = \frac{d}{dt}B(t) = \frac{df}{dy}\cdot B(t) + \frac{df}{dPar} \tag{13}$$

In Eq. (12), $B(t)$ defines the sensitivity function for each model response with respect to the model parameters. In Eq. (13) it can be seen that defining sensitivities as a function of time allows them to be solved alongside the main system differential equations, improving solver efficiency and performance.

To minimise cross-correlation between the energy (activation energy, E_a or equilibrium adsorption energy, ΔH_{ads}) and pre-exponential factor (A_i) parameters, a re-parameterised Arrhenius or Van't Hoff equation was used:

[2] Athena Visual Studio 14.2, Stewart & Associates Engineering Software, Inc.

Table 4
Standard catalyst precursor reduction procedure employed in this study.

Step	Gas	Set point (K)	Ramp rate (K h^{-1})	Flow rate (L h^{-1})	Pressure (bar)	Dwell (h)
1.	2% H_2/N_2	363	120	7.5	10	0
2.	2% H_2/N_2	408	60	7.5	10	0
3.	2% H_2/N_2	498	30	7.5	10	1
4.	2% H_2/N_2	473	60	7.5	25	6

$$k_i = A_{i,473} \cdot \exp\left(\left(\frac{E_a}{T_{base} \cdot R}\right) \cdot \left(1 - \frac{T_{base}}{T}\right)\right) \quad (14)$$

$$K_i = A_{i,473} \cdot \exp\left(\left(\frac{\Delta H_{ads}}{T_{base} \cdot R}\right) \cdot \left(1 - \frac{T_{base}}{T}\right)\right) \quad (15)$$

where base temperature, T_{base} = 473 K and $A_{i,473}$ is the value of the rate constant k_i or K_i at 473 K. 473 K is chosen as this temperature was used during initial isothermal analysis of each of the candidate kinetic models. Hence, this provides an accurate initial prediction for the A_i parameters during the multi-temperature data fitting stage, thus facilitating a more accurate estimation of E_a or ΔH_{ads} parameters.

The fitting process is further improved by solving $A_{i,373}$ as an exponential term and lumping fitted value, E_a or ΔH_{ads} with constants T_{base} and ideal gas constant, R (J K^{-1} mol^{-1}) to give fitting parameter $E_{a,lump}$ or $\Delta H_{ads,lump}$. This typically brings the values of $A_{i,373}$ and $E_{a,lump}$ or $\Delta H_{ads,lump}$ into the same order of magnitude (typically ±1–10) further reducing cross-correlation in this expression:

$$k_i = \exp\left(A_{i,473} + \left(E_{a,lump} \cdot \left(1 - \frac{T_{base}}{T}\right)\right)\right) \quad (16)$$

$$K_i = \exp\left(A_{i,473} + \left(\Delta H_{ads,lump} \cdot \left(1 - \frac{T_{base}}{T}\right)\right)\right) \quad (17)$$

Thermodynamic equilibrium constants, taken from Graaf and co-workers [39], were utilised in all kinetic equations to account for thermodynamic limitations. The values for these are calculated as follows:

$$CO_2 + 3H_2 \underset{k_{-1}}{\overset{k_1}{\Longleftrightarrow}} CH_3OH + H_2O = \log_{10} K_1^* = \frac{-3066}{T} + 10.592 \quad (18)$$

$$CO_2 + H_2 \underset{k_{-2}}{\overset{k_2}{\Longleftrightarrow}} CO + H_2O = \log_{10} K_2^* = \frac{2073}{T} - 2.029 \quad (19)$$

$$CO + 2H_2 \underset{k_{-3}}{\overset{k_3}{\Longleftrightarrow}} CH_3OH = \log_{10} K_3^* = \frac{-5139}{T} + 12.621 \quad (20)$$

Gaseous components were also checked for non-ideal behaviour. This was achieved by using the Soave–Redlich–Kwong equation of state [40], which takes the following form:

$$Z = Pv/RT = \frac{v_m}{v_m - b} - \frac{a(T)}{RT(v + b)} \quad (21)$$

where Z is compressibility factor, P is total pressure (bar), v_m is molar volume (m^3 mol^{-1}), R is gas constant (J mol^{-1} K^{-1}), and a (–) and b (m^3 mol^{-1}) are constants taken from the literature [39]. Across all data generated in the experimental programme, Z never exceeded the bounds of $0.99 < Z < 1.01$. Hence the use of partial pressures, rather than fugacities, is acceptable for this kinetic study.

3. Results and discussion

In order to tackle the objectives given in Section 1.2, the results and discussion for this study are divided into five sections. Firstly, the initial precursor reduction step will be firstly examined for Cu/ZnO/Al_2O_3 catalysts (Section 3.1). Following this, steady and non-steady state kinetics under $CO/CO_2/H_2$ conditions for this catalyst will be explored (Sections 3.2.1–3.2.3). The understanding of catalyst functionality under each of these feeds will then be applied to binary (Cu/ZnO and Cu/Al_2O_3) formulations (Section 3.3).

3.1. Initial reduction of $CuO/ZnO/Al_2O_3$

In all experiments carried out in this study, the catalyst precursors were initially reduced under a flow of 2% H_2/N_2. Table 4 shows the standard procedure which was applied to all catalyst beds during the reduction step. This reduction procedure applies to all catalyst masses tested in the study (e.g. 0.125, 0.250, 0.375 and 0.5 g).

It is important to analyse the gaseous products from this reduction step in order to understand the transformations that the catalyst precursor undergoes in delivering a catalyst in the 'active' state for methanol synthesis. This will also provide a reference state for the catalyst prior to exposure to $CO/CO_2/H_2$ conditions.

Fig. 2A and B shows the product H_2O and CO_2 evolved, respectively, during the reduction step across $CuO/ZnO/Al_2O_3$ catalyst beds of different mass using the parallel difference test configuration. It can be seen that both H_2O and CO_2 are evolved in a 'wave-like' fashion along the catalyst bed. It is well known in the literature that the evolution of H_2O during this reduction step is largely due to the reduction of copper(II) oxide (CuO) to copper metal (Cu^0) [41], which occurs under mild temperatures and reducing conditions. At temperatures below 373 K, H_2O evolution may also be attributed to physisorbed moisture in the sample. The CO_2 evolved can be attributed to decomposition of metal hydroxy-carbonates (e.g. $Cu_2(OH)_2CO_3$) which were not removed in prior catalyst precursor formulation steps (e.g. calcination) [42]. It is important to note that whilst ZnO is a reducible component, it is highly unlikely that it is reduced under the applied reduction conditions. This has been demonstrated previously in the literature [41].

Based on structural compositions of the initial $CuO/ZnO/Al_2O_3$ sample, the volumes of H_2O and CO_2 observed can be linked to specific mass losses in the sample. In Table 5, the measured oxygen mass loss calculated from product H_2O is very similar to the calculated mass of oxygen in the CuO component of the catalyst precursor. This suggests that this component is almost entirely reduced to Cu^0 by the end of the reduction step.

3.2. Experimental and kinetic analysis of $Cu/ZnO/Al_2O_3$ under $CO/CO_2/H_2$ feeds

3.2.1. Steady state experimental

Following the reduction step described in Section 3.1, $Cu/ZnO/Al_2O_3$ catalysts were tested under steady state conditions. The testing was carried out in parallel difference mode (bed masses: 125, 250, 375 and 500 mg). All catalyst beds were initially exposed to 3% CO/3% CO_2/67% H_2/27% N_2 gas at 25 bar and 473 K for 10 h, during which time steady state behaviour was observed. Subsequently, all catalyst beds were cycled through a variety of conditions:

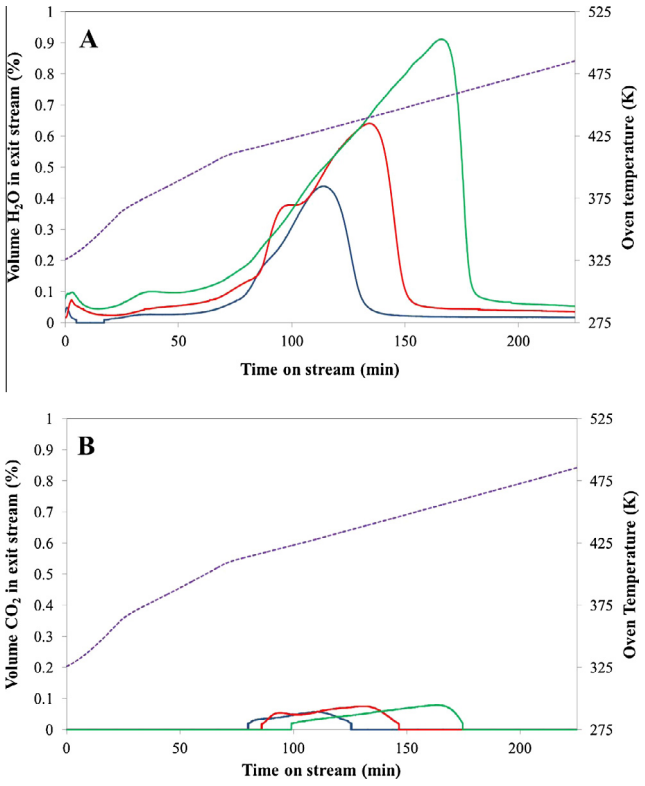

Fig. 2. Evolution of (A) H_2O and (B) CO_2 during the initial $CuO/ZnO/Al_2O_3$ reduction step under 2% H_2/N_2 at 10 bar. (—) denotes 125 mg bed, (—) 250 mg bed, (—) 500 mg bed and (--) oven temperature (K).

Table 5
Comparison of measured mass losses of $CuO/ZnO/Al_2O_3$ during reduction with calculated values.

	Initial mass of catalyst		
	125 mg	250 mg	500 mg
Measured mass of oxygen lost from catalyst (based on H_2O eluted) (mg)	17	33	60
Calculated mass of oxygen in CuO component of initial precursor sample (mg)	15	30	60

- 3 different feed gases (CO/CO_2 % varied: 3:3, 3:1. 3:0.3)
- 5 temperatures (453, 463, 473, 483, 493 K)
- 3 pressures (15, 25, 35 bar)

In total 33 distinct set point observations were made for each of the four catalyst beds and blank reference reactor. These observations were made in a randomised order with periodic checks made at the reference condition in order to confirm that the catalyst had not intrinsically changed in activity. Each catalyst bed was exposed to each set point for a minimum 3 h allowing multiple readings and confirmation of stability to be obtained. An example of such a procedure is shown in Fig. 3. Intrinsic activity losses never exceeded 5% throughout the steady state testing program, confirming earlier calculations. This was ensured by regularly returning the catalyst performance to reference conditions (473 K, 25 bar, $CO/CO_2/H_2/N_2$ (3/3/67/27)).

The final dataset of 165 distinct observations, each containing four responses (CO, CO_2, CH_3OH, H_2O) can be found in Supplementary Information. An example of catalyst steady state performance is shown in Fig. 4. In these three graphs the $Cu/ZnO/Al_2O_3$ catalyst is exposed to 25 bar, 473 K conditions under the three different feed gases. By using the outlet responses from all four catalyst beds, a set of axial concentration profiles are observed.

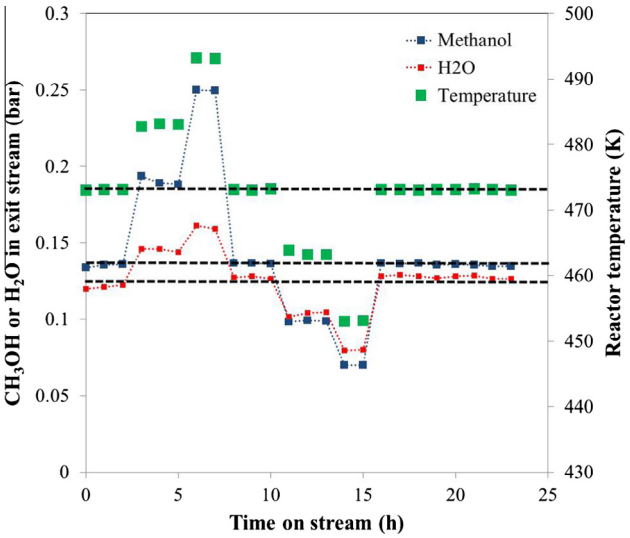

Fig. 3. Catalyst stability example during steady state testing. Conditions: Feed $CO/CO_2/H_2/N_2$ (3/3/67/27), flow rate 7.5 L h^{-1}, 500 mg $Cu/ZnO/Al_2O_3$ catalyst.

In Fig. 4A, apparent CO_2 consumption occurs in the first sector of the catalyst bed but reaches a steady value thereafter. CO behaves in the exact opposite manner and is consumed in sectors 2–4. H_2O is only produced in the first sector and also reaches a steady level in the subsequent sectors. Use of Eq. (18) reveals that the equilibrium composition for the RWGS is reached under these conditions and explains the steady levels of CO_2 and H_2O in sectors 2–4. CH_3OH production increases with axial distance along the reactor (0.93 and 1.12 μmol s^{-1} g^{-1} in the 1st and 4th sectors respectively). These values are consistent with the observations of Sahibzada and co-workers [8] who found that CH_3OH production rates were greater under integral 'finite' conversion compared to differential conversion in $CO_2/(CO + CO_2)$ feed inlet values of less than 0.2.

In Fig. 4B, a higher CO_2 content in the inlet feed results in CO_2 consumption being observed in the 1st and 2nd sectors before reaching a steady level. This is again mirrored by H_2O production. The levelling off of both gas phase species can again be attributed to the equilibrium composition of the RWGS reaction being reached. Again CO consumption appears to replace CO_2 consumption in the back sectors of the catalyst bed. CH_3OH production rates are greatest in the 1st sector of the reactor and slowly retard along the reactor (0.97 and 0.73 μmol h^{-1} g^{-1} in the 1st and 4th sectors respectively). This again agrees with [8] for a $CO_2/(CO + CO_2)$ feed inlet values of 0.25.

In Fig. 4C, CO_2 consumption is observed along the complete axial length of the reactor. The equilibrium composition for the RWGS reaction is approached but is not reached, owing to the shift in this value from the increased CO_2 content in the inlet feed. CH_3OH production rates are considerably higher at the front of the reactor compared to the back (1.34 and 0.81 μmol h^{-1} g^{-1} in the 1st and 4th sectors respectively). This again agrees with [8] for a $CO_2/(CO + CO_2)$ feed inlet values of 0.5.

The observations in Fig. 4 are indicative of the general trends seen in the wider dataset. In general, it appears that CO_2 consumption is gradually replaced by CO consumption along the reactor as the RWGS equilibrium compositions are reached. This replacement does not lead to a sharp loss in CH_3OH productivity. At face value, this would suggest CO becomes the source of carbon in CH_3OH production along the reactor; a route which was supported by earlier works [44,12,43]. However it was earlier discussed that the $CO_2 \rightarrow CH_3OH$ route has been demonstrated to be considerably faster than the CO route over a $Cu/ZnO/Al_2O_3$ catalyst and is key to maintaining CH_3OH activity [6,7,9,14]. Hence a more detailed steady state model may be required to describe this behaviour.

In the discussion of Fig. 4A–C, it was noted that the equilibrium mixture for the RWGS reaction is reached at different stages along the axial length of the reactor, depending on feed, temperature and pressure. Indeed, for all three reactions described in Eqs. (18)–(20), proximity to equilibrium mixtures should be analysed and utilised in the subsequent kinetic model. To illustrate, an overall 'equilibrium term', β_i^*, which comprises both a thermodynamic constant, K_i^* (based on [39]) and driving force (partial pressures) of the gases in the forward and backward direction of each reaction of interest can be calculated:

$$\text{For } CO_2 \rightarrow CH_3OH: \quad \beta_1^* = K_1^* \frac{p_{CH_3OH} p_{H_2O}}{p_{CO_2} p_{H_2}^3} \tag{22}$$

$$\text{For } CO_2 \rightarrow CO: \quad \beta_2^* = K_2^* \frac{p_{CO} p_{H_2O}}{p_{CO_2} p_{H_2}} \tag{23}$$

$$\text{For } CO \rightarrow CH_3OH: \quad \beta_3^* = K_3^* \frac{p_{CH_3OH}}{p_{CO} p_{H_2}^2} \tag{24}$$

Fig. 5A and B illustrates the overall magnitude of the 'equilibrium term' at axial sector outlets for both the $CO_2 \rightarrow CH_3OH$ and $CO_2 \rightarrow CO$ reaction respectively, for all steady state conditions tested. A β_i^* value of exactly 1 implies a particular reaction is at thermodynamic equilibrium. For the $CO_2 \rightarrow CH_3OH$ reaction in Fig. 5A, all conditions tested favour the forward reaction to methanol. The largest value of β_1^* across the entire dataset is 0.5 at the 4th sector outlet under conditions of 15 bar, 493 K. Hence thermodynamic limitations should be considered when testing kinetic models for this reaction but a full kinetic description to describe the back reaction, $CH_3OH \rightarrow CO_2$ is not necessary.

In Fig. 5B, describing the equilibrium term for the $CO_2 \rightarrow CO$ reaction, a distinct trend is seen. The outlet equilibrium terms in the 1st sector are predominantly on the side of favouring RWGS ($\beta_2^* < 1$) whilst the 2nd – 4th sectors are predominantly on the other side of the equilibrium term ($\beta_2^* > 1$), favouring the FWGS reaction. In a number of cases, the β_2 term is significantly higher than 1, which would lead to the FWGS reaction taking place under kinetic control. Hence, across the steady state dataset it may not be sufficient to describe WGS catalysis by one reaction with a thermodynamic equilibrium term. A kinetic expression for both the FWGS and RWGS reactions is likely needed and will be modelled in Section 3.2.2.

3.2.2. Steady state kinetic modelling

In this section the data described in Section 3.2.1 were tested against the four Langmuir–Hinshelwood type models described in Table 1. Additionally, the methanol synthesis and reverse water gas shift reactions were also tested using an empirical power law relationship as a base case:

$$r_1 = k_1 P_{CO}^{a1} P_{CO_2}^{a2} P_{H_2}^{a3} P_{H_2O}^{a4} P_{CH_3OH}^{a5} (1 - K_1^* (P_{MeOH} P_{H_2O}) / (P_{CO_2} P_{H_2}^3)) \tag{25}$$

$$r_2 = k_2 P_{CO}^{b1} P_{CO_2}^{b2} P_{H_2}^{b3} P_{H_2O}^{b4} P_{CH_3OH}^{b5} (1 - K_2^* (P_{CO} P_{H_2O}) / (P_{CO_2} P_{H_2})) \tag{26}$$

where *a1–a5* and *b1–b5* are empirical apparent order fitting parameters. The procedure carried out in this section is as follows:

1. Test the entire dataset (152 experimental observations) using the power law and Langmuir–Hinshelwood models. Carry out initial model discrimination based on quality of prediction and parameter estimations.
2. Test two datasets using the remaining model candidates which are discretised by the water gas shift equilibrium position at the inlet to the catalyst bed sector under consideration:
   a. RWGS dataset (44 observations): referred to as $\beta_2^* < 1$ dataset
   b. FWGS dataset (108 observations): referred to as $\beta_2^* > 1$ dataset

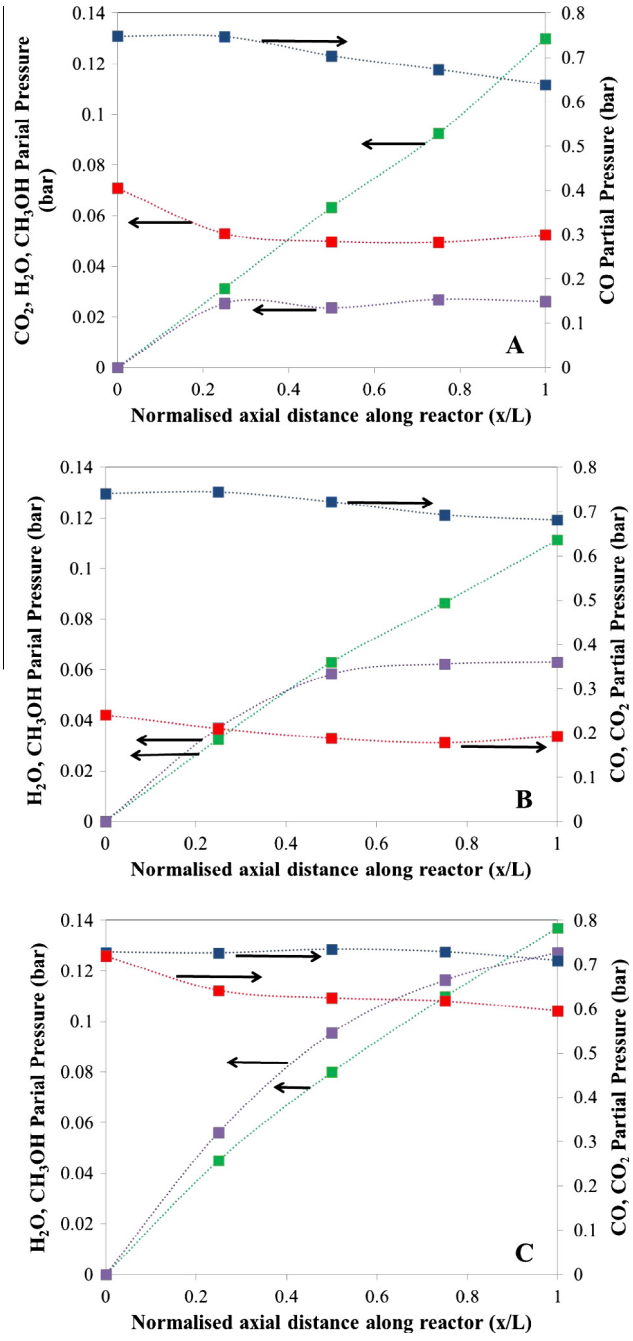

Fig. 4. Steady-state axial concentration plots for a $Cu/ZnO/Al_2O_3$ catalyst operating under 473 K, 7.5 L h^{-1} conditions with CO/CO_2 inlet ratios of (A) 10:1, (B) 3:1 and (C) 1:1. Symbols denote: (■) CO, (■) CO_2, (■) CH_3OH and (■) H_2O. Lines are to guide the eye.

3. Select best candidate model based on physic-chemical consistency between the model predictions in each of the two datasets.

Analysis from step 1 can be found in Supplementary Information. The models of Graaf and co-workers [12], Mochalin and co-workers [9] and Vanden Bussche and Froment [14] were found to all be potentially suitable models at this round of discrimination. The model of Coteron and Hayhurst [20] returns a poor fit and set of parameter estimates and was discounted. Additionally, the power law model suggests that FWGS could play a significant role

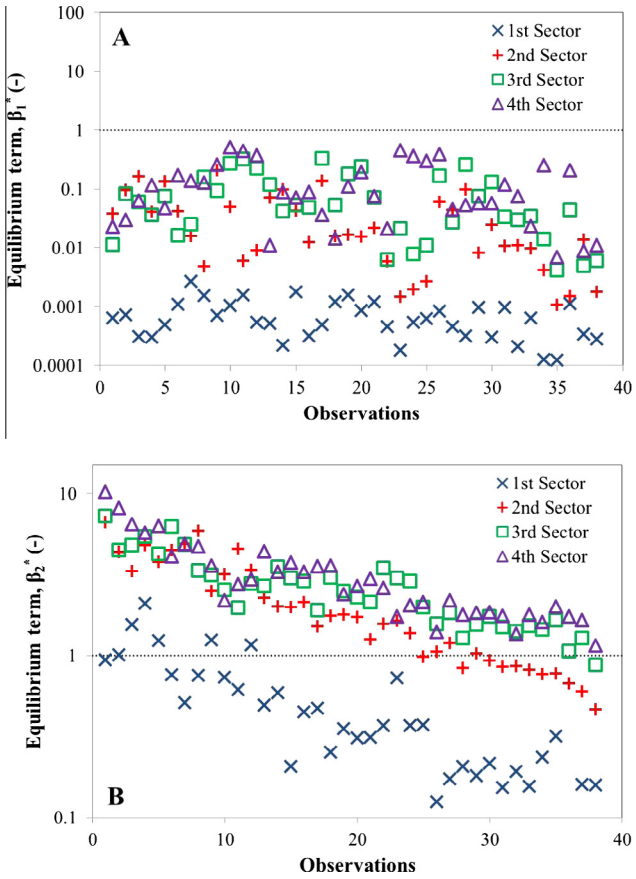

Fig. 5. Values of equilibrium terms (A) β_1^* and (B) β_2^* at individual sector outlets for all experimental steady state data points in the study.

in the reaction kinetics over this catalyst. Hence the second stage of kinetic model testing was carried out where the dataset was discretised into two sets for the remaining model candidates. For the $\beta_2^* > 1$ dataset, rate equation r_2 (RWGS) was exchanged for r_4 (FWGS) in each case:

$$r_4 = \frac{k_4 P_{CO} P_{H_2O}\left(1 - \frac{1}{K_2^*}(P_{CO_2}P_{H_2})/(P_{CO}P_{H_2O})\right)}{\left(1 + K_{redox}\frac{P_{H_2O}}{P_{H_2}} + \sqrt{K_{H_2}P_{H_2}} + K_{H_2O}P_{H_2O} + K_{CO_3}P_{CO_2}\sqrt{P_{H_2}} + K_{HCO_2}\frac{P_{CO_2}P_{H_2O}}{P_{H_2}}\right)} \quad (27)$$

$$r_4 = \frac{k_4 P_{CO} P_{H_2O}\left(1 - \frac{1}{K_2^*}(P_{CO_2}P_{H_2})/(P_{CO}P_{H_2O})\right)}{(P_{CO_2} + K' P_{CO_2} P_{H_2O} + K'' P_{H_2O})} \quad (28)$$

$$r_4 = \frac{k_4 K_{CO}\left(P_{CO}P_{H_2O} - \frac{P_{CO_2}P_{H_2}}{K_2^*}\right)}{(1 + K_{CO}P_{CO} + K_{CO_2}P_{CO_2})\left(P_{H_2}^{1/2} + \frac{K_{H_2O}P_{H_2O}}{K_{H_2}^{1/2}}\right)} \quad (29)$$

where Eqs. (27)–(29) describe the FWGS descriptions for the models of Vanden Bussche and Froment, Mochalin and co-workers, and Graaf and co-workers, respectively [9,12,14]. The adsorption constants in each model remain the same. The basis here is that the FWGS reaction proceeds via the same set of steps as in RWGS, except in the opposite direction for each mechanistic model.

Fig. 6 provides a comparison of the total residuals of all four model responses in the case that the full dataset is modelled in one expression, or if it is split based on WGS reaction equilibrium position. In both the Vanden Bussche and Froment [14] and Mochalin and co-workers [9] models there is a significant reduction in the residuals for CO and CH_3OH responses. These are the key species which are consumed and produced respectively in

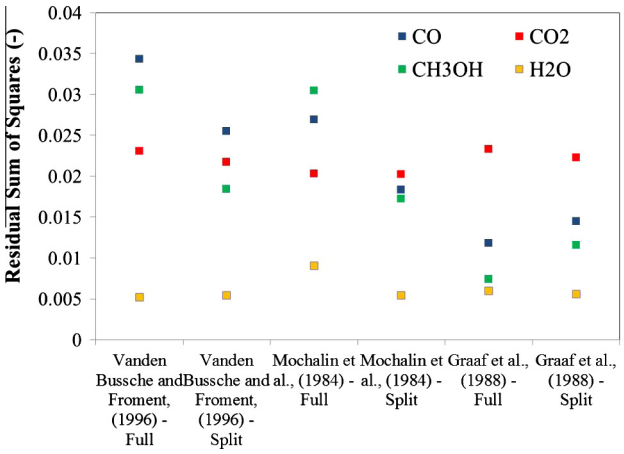

Fig. 6. Comparison of total residual sum of squares for each model response using the single model or split model approach for the three remaining Langmuir–Hinshelwood models under consideration. All 152 experimental observations were used in this analysis.

the $\beta_2^* > 1$ section of the dataset. The model of Graaf and co-workers [12] on the other hand has a poor prediction for both CO and CH_3OH upon splitting the models.

In Table 6, the parameter estimates and condition numbers for the discretised models are shown. The condition number value in this table is calculated as follows:

$$\kappa_{CC} = \|CC\| \cdot \|CC^{-1}\| \quad (30)$$

where κ_{CC} is the condition number and CC is the cross correlation matrix between the parameters in the kinetic model under consideration.

The model splitting approach to the analysis reveals some inconsistencies in some of the models. In Mochalin and co-workers [9] the K' term is positive in the $\beta_2^* < 1$ dataset. This is fundamentally incorrect as adsorption equilibrium terms must have a negative sign. This is particularly concerning as it is present in the RWGS description, which was the basis for the original model development. A dramatic shift from 148 to 33 kJ mol^{-1} for the methanol synthesis rate constant in the two datasets also makes very little sense unless the rate determining step for the reaction has changed as a function of conditions along the reactor.

Concerning the model of Graaf and co-workers [12] the $\beta_2^* < 1$ dataset contains both indeterminate parameters and a RWGS activation energy with a confidence interval that is close to 100% of the estimated value. Meanwhile, with the $\beta_2^* > 1$ dataset, key issues in the prediction are strong cross correlation of parameters evidenced by a very high condition number and poor confidence intervals for all pre-exponential factors. Also a significant shift is seen from 46.7 to 81.8 kJ mol^{-1} for the methanol synthesis reaction activation energy. This implies a different rate determining step based on the dataset used.

The model of Vanden Bussche and Froment [14] is the only one of three models to show consistency in the datasets on either side of the WGS equilibrium line. The estimated E_a values for methanol synthesis are 99 and 118 kJ mol^{-1} and are close to indiscriminate once confidence intervals are considered. Additionally, the K_{redox} and K_{CO3} adsorption terms are dominant in both datasets. Adsorption strength of both is estimated to be lower in the $\beta_2^* > 1$ dataset. This is logical as the switch to FWGS will promote removal of O.s sites in the CO + O.s → CO_2 step of the reaction which would correlate with a K_{redox} reduction and less O.s to assist in carbonate formation. However the significance of these differences is speculative as the estimated adsorption constants are indiscriminate once confidence intervals are considered. The confidence

Table 6
Estimated parameters and calculated condition numbers for the remaining three Langmuir–Hinshelwood models under consideration. Results are discretised into the $\beta_2^* < 1$ and $\beta_2^* > 1$ datasets. Confidence intervals are 95% higher probability density intervals calculated from the Bayesian estimation procedure.

Parameter		Kinetic model					
		Vanden Bussche and Froment [14])		Mochalin et al. [9]		Graaf et al. [12]	
Dataset		$\beta_2^* < 1$	$\beta_2^* > 1$	$\beta_2^* < 1$	$\beta_2^* > 1$	$\beta_2^* < 1$	$\beta_2^* > 1$
k_1	$A_{i,473K}$	0.086 ± 0.052	0.131 ± 0.035	0.026 ± 0.006	0.069 ± 0.010	22.7 ± 2.32	0.615 ± 0.511
	E_a	99.0 ± 16.6	118 ± 8.58	148 ± 21.1	33.0 ± 15.3	46.7 ± 10.2	81.8 ± 3.82
k_2 or k_4	$A_{i,473K}$	0.142 ± 0.720	2.67 ± 0.340	0.009 ± 0.007	5.05 ± 0.721	65.6 ± 27.7	225 ± 180
	E_a	188 ± 71.9	106 ± 11.3	186 ± 58.5	74.9 ± 15.6	43.6 ± 43.0	129 ± 9.63
K_{redox}	$A_{i,473K}$	236 ± 182	186 ± 49.2	–	–	–	–
	ΔH_{ads}	–	–	–	–	–	–
K_{CO3}	$A_{i,473K}$	0.172 ± 0.072	0.130 ± 0.064	–	–	–	–
	ΔH_{ads}	–	–	–	–	–	–
K'	$A_{i,473K}$	–	–	61.3 ± 24.3	137 ± 28.2	–	–
	ΔH_{ads}	–	–	96.4 ± 37.6	−103 ± 22.3	–	–
K_{CO}	$A_{i,473K}$	–	–	–	–	229 ± 223	–
	ΔH_{ads}	–	–	–	–	−160 ± 59.7	–
K_{CO2}	$A_{i,473K}$	–	–	–	–	Indet.	133 ± 115
	ΔH_{ads}	–	–	–	–	–	–
Condition number		432	472	158	214	34	18,111

intervals of the parameters are in general much better for the $\beta_2^* > 1$ dataset, owing to the larger amount of data in this set. However, the condition numbers are similar for both models, thus implying similar model stability.

The use of dataset discretisation based on WGS equilibrium values has acted as an additional model discrimination tool. The only model showing phenomenological consistency between each dataset is that of Vanden Bussche and Froment [14]. As a model based on micro kinetics, this emphasises the strength in considering all reaction steps in model construction. The basis of this model will be utilised in considerations for the non-steady state investigations in the following section. Parity plots for the full and discretised dataset models can be found in Supplementary Information (Figs. S2 and S3).

3.2.3. Non-steady state investigations

In addition to developing a steady state kinetic model under $CO/CO_2/H_2$ conditions, understanding the approach to steady state performance of a $Cu/ZnO/Al_2O_3$ catalyst during start-up provides insight into the generation of methanol synthesis and WGS activity on the catalyst surface. Start-up under $CO/CO_2/H_2$ is shown in Fig. 7.

Both profiles in Fig. 7 show an immediate consumption of CO_2 upon breakthrough of the $CO/CO_2/H_2$ gas at $t = 0$ min. The majority of this consumption is in the front 250 mg of the catalyst bed. Consumption of CO is not observed initially, and only in notable levels across the 500 mg bed from $t = 5$ min onwards. Water production is increasingly observed from $t = 0$ min, whilst methanol production is not seen until $t = 2.5$ min in both beds.

This suggests that RWGS takes place from $t = 0$ min whilst the methanol synthesis reaction is delayed. It is important to note that the initial copper surface under these conditions is assumed to be completely reduced, based on calculations in Section 3.1. In the kinetic model proposed in Section 3.2.2, the following initial steps are prevalent for methanol synthesis and RWGS respectively:

$$CO_2(g) + s. + O.s \Longleftrightarrow CO_3.2s \quad (31)$$

$$CO_2(g) + s \Longleftrightarrow CO(g) + O.s \quad (32)$$

where $CO_3.2s$ is carbonate species adsorbed to two copper sites. Hence, on an initially reduced copper surface it is feasible to assume that the methanol synthesis initiation step in Eq. (31) is not possible until a population of O.s sites has built up via Eq. (32). To further explore, the carbon and oxygen balances over both catalyst beds were determined and were found to be significantly less than 100% initially.

Fig. 8 shows a cumulative plot for missing moles of 'C' and 'O' over the first 30 min time on stream for both catalyst beds. Further

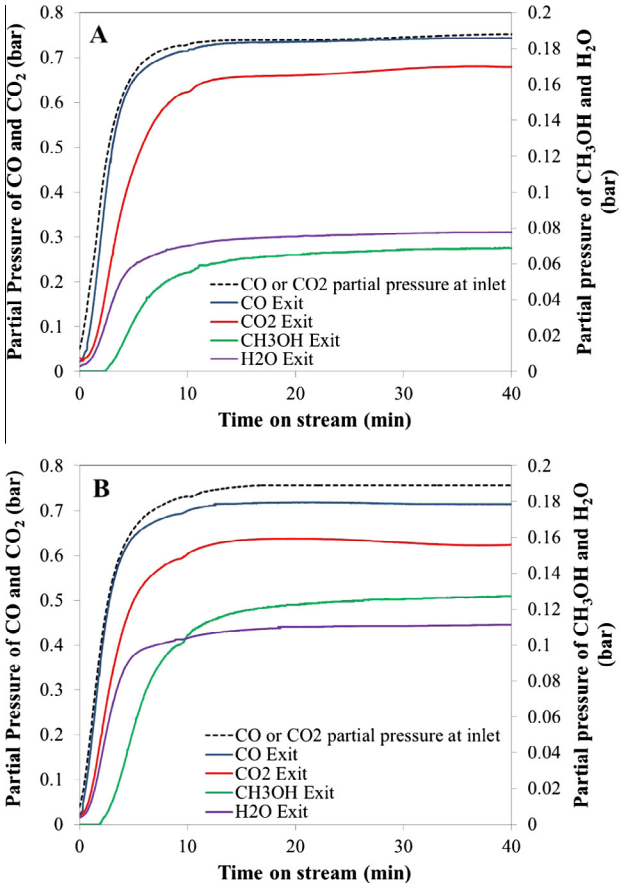

Fig. 7. Reaction performance of (A) 250 mg, (B) 500 mg of $Cu/ZnO/Al_2O_3$ catalyst upon feeding $CO/CO_2/H_2/N_2$ (3:3:67:27) at 7.5 L h^{-1} (STP) at 25 bar, 473 K. The catalyst had undergone reduction in 2% H_2/N_2 as shown in Section 3.1 prior to this exposure.

small increases in missing carbon and oxygen were seen after this time but cannot be reasonably discriminated due to experimental error in the rig.

In Fig. 8, missing oxygen is always greater than carbon in both the 250 and 500 mg beds. It is very clear, however, that the majority of the missing species are located in the front 250 mg of the catalyst bed. After 30 min operation, 260 ± 21 μmol of carbon species are present on the front 250 mg of the catalyst bed compared to

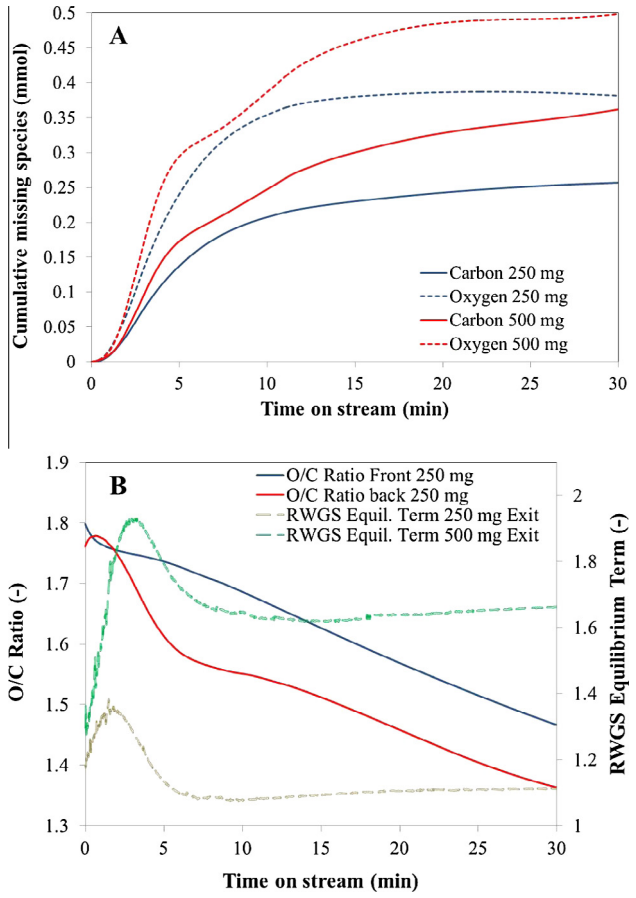

Fig. 8. (A) Cumulative missing carbon and oxygen over a $Cu/ZnO/Al_2O_3$ catalyst during the first 30 min operation under $CO/CO_2/H_2/N_2$ (3:3:67:27) at 7.5 L h^{-1} (STP) at 25 bar, 473 K. (B) Calculated O/C ratio and RWGS equilibrium term at bed exits.

100 ± 36 μmol in the back 250 mg (error bars assuming 5% error in all experimental measurements). Assuming these species have molecular size similar to that of CO_2 (3.3 Å), this leads to a surface coverage of 41 and 16 $m^2\ g^{-1}$ (based on as reduced weight) for each 250 mg sector respectively. Both of these estimated values are within range of the copper surface area of the catalyst (41.1 $m^2\ g^{-1}$ based on reduced weight).

Corresponding methanol productivity over each sector after 30 min was 1.05 and 0.89 μmol $s^{-1}\ g^{-1}$ which would correspond to less than 0.4% and 0.9% of the carbon surface population respectively. Hence there appears to be no direct link between overall carbon coverage and methanol productivity.

The overall missing oxygen to carbon (O/C) ratio is also shown for the first 30 min on stream in Fig. 8B. Initially, this ratio is ~1.8 in both 250 mg sections of the bed suggesting that the majority of adsorbed species likely originate from CO_2. This ratio subsequently declines slowly in the front 250 mg and much more quickly in the back 250 mg to values of 1.45 and 1.36 respectively after 30 min. The dynamic changes in this ratio appear to coincide with changes in the position of the RWGS equilibrium term. The term rapidly increases between 0 and 4 min, particularly at the 500 mg exit. This suggests that the direction of the reaction has switched towards FWGS, resulting in a relative loss of oxygen from the catalyst surface. The significant carbon coverage, with >1 O/C ratio observed does however provide support for the presence of a significant number of species containing two oxygen atoms. In the micro kinetic molecule, this would point to populations of carbonates and formates, the former of which is featured as a significant adsorption constant in the steady state kinetic model.

A further, simple analysis can be made on the front 250 mg of the catalyst bed by examining the rate of water production from RWGS, using the following assumption:

$$\text{Mol } H_2O \text{ from RWGS} = \text{Mol } H_2O \text{ at 250 mg bed exit} - \text{Mol } CH_3OH \text{ at 250 mg bed exit} \quad (33)$$

In Eq. (33), moles of methanol observed at the bed exit act as a representation of the number of moles of water formed as a result of methanol synthesis from CO_2. The results for this over the first 15 min of operation are shown in Fig. 9.

Water productivity from RWGS is compared to the molar rate at which oxygen is lost from the feed. Both profiles follow a similar pattern, albeit there is a small delay between the rate of oxygen loss from the feed and that of water production from RWGS. This shows a direct link between oxygen lost from the feed to the catalyst surface and the RWGS reaction. Eq. (30), which denotes the dissociation of CO_2 over a vacant site, is the rate determining step for the RWGS in the steady state model of this study and in previous literature [14]. With this mechanism in mind, the delay in the two profiles may relate to this step following initial adsorption of CO_2 onto the catalyst surface. As the rate of oxygen lost from the feed drops in Fig. 9, so does the rate of RWGS. This suggests that an increased build-up of oxygen (O.s type) species retards RWGS which is logical based on Eq. (32) and stresses the importance of a redox balance on the catalyst surface for this mechanism.

3.3. Binary formulations under steady state operation

Reaction testing of binary formulations was utilised to provide further understanding of copper-based catalyst functionality under $CO/CO_2/H_2$ conditions. In Table 7, the reduction step and productivity of all three catalysts under reaction conditions are compared.

As with the $CuO/ZnO/Al_2O_3$ catalyst precursor formulation, both the CuO/ZnO and CuO/Al_2O_3 catalysts released an amount of oxygen during the reduction step (as H_2O) that was almost equivalent to the oxygen content of CuO in the sample. This again suggests that the entire copper component is reduced to Cu^0 during this procedure. All three catalysts were subsequently tested under steady state $CO/CO_2/H_2$ conditions at 473 K, 25 bar. Methanol productivity over a 500 mg bed followed the trend of $Cu/ZnO/Al_2O_3$ > Cu/ZnO > Cu/Al_2O_3, which can be linearly correlated with the copper metal surface area of each of these three formulations, agreeing with previous literature [7]. Any correlation for RWGS and/or FWGS productivity is less clear from these data however

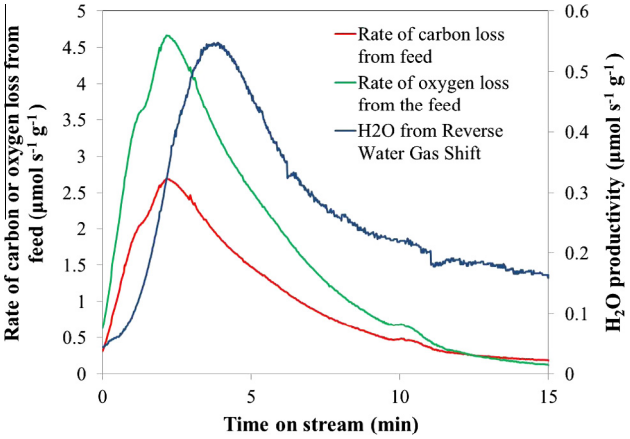

Fig. 9. Comparison on H_2O productivity and rate of carbon and oxygen lost over the front 250 mg of a $Cu/ZnO/Al_2O_3$ catalyst bed during the first 15 min operation under $CO/CO_2/H_2/N_2$ (3:3:67:27) at 7.5 L h^{-1} (STP) at 25 bar, 473 K.

Table 7
Comparison of binary and ternary copper-based formulations during reduction step and under $CO/CO_2/H_2$-feed reaction conditions (N.B.: values relate to a catalyst precursor charge of 500 mg).

Catalyst precursor	Calculated oxygen within CuO component of precursor (mg)	Measured oxygen released during 2% H_2/N_2 reduction	Steady state productivity at 473 K, 25 bar[a] ($\mu mol\ g^{-1}\ s^{-1}$)	
			CH_3OH	H_2O
$CuO/ZnO/Al_2O_3$	60	60	1.04	0.89
CuO/ZnO	34	36	0.44	0.59
CuO/Al_2O_3	25	26	0.06	0.37

[a] Feed gas employed was $(CO/CO_2/H_2/N_2) = (3/3/67/27)$ at 7.5 L h^{-1}.

Table 8
Application of steady state parallel difference test data for binary and ternary copper-based formulations under reaction conditions using the kinetic model developed in this study.[a,b]

Model parameter	$Cu/ZnO/Al_2O_3$	Cu/ZnO	Cu/Al_2O_3
k_1	0.086 ± 0.052	0.010 ± 0.002	0.002 ± 0.001
k_2	0.142 ± 0.072	0.145 ± 0.072	0.157 ± 0.056
K_{redox}	236 ± 182	154 ± 26.0	414 ± 313
K_{CO3}	0.172 ± 0.072	Neg.	Neg.

[a] Conditions $(CO/CO_2/H_2/N_2) = (3/3/67/27)$ at 7.5 L h^{-1}, 473 K, 25 bar.
[b] R^2 values for all individual model responses were >0.99 for all three datasets.

and requires a cross-check with the steady state model developed earlier in this study.

Table 8 shows the fitted rate constant parameters for all terms in the steady state model of this study, using parallel difference test data at 25 bar, 473 K, for all three formulations:

In Table 8, all sector data have inlet β_2^* values of less than one and so the $\beta_2^* < 1$ model was applied. The k_1 values for each catalyst follow the overall methanol synthesis productivity trend. However, where the overall productivity and copper surface area correlation is roughly linear, the productivity relationship is non-linear with the rate constant. For example $Cu/ZnO/Al_2O_3$ has a rate constant magnitude 8.6 times that of Cu/ZnO but the productivity difference is only 2.4 times.

Meanwhile, a comparison of all three k_2 values shows negligible differences in RWGS activity between the formulations (within the confidence intervals of the parameters). In previous literature [23], it was found that WGS activity of copper-based formulations was not linked to copper metal surface area, as the current study also suggests. Similarly, no correlation based on support choice can be made from these estimates.

It is difficult to ascribe a correlation between the K_{redox} values of the catalysts due to the wide confidence intervals; however, the importance of the O.s vs. s balance between these catalysts in determining methanol synthesis activity cannot be discounted. For each catalyst however, this is clearly an important term and further investigation into the link between redox balance and methanol synthesis activity on these surfaces would be informative.

Neither of the binary formulations returned an estimated parameter for carbonate adsorption. For the Cu/ZnO an indeterminate value of 0.02 was returned, whilst for the Cu/Al_2O_3 the value was infinitesimally small. Tenuously, the prevalence of this parameter may follow methanol synthesis productivity and hence copper surface area. The formation of carbonates requires a bidentate mode of adsorption on copper. Hence the lower the surface area of copper, the lower the likelihood there is of this adsorption mode taking place.

4. Conclusions

The overall aim of this work was to provide a new perspective on the steady and non-steady state kinetics of Cu-based methanol synthesis catalysts under $CO/CO_2/H_2$ using reactor discretisation methods. Such approaches are not commonly used in the literature, particularly under integral, elevated pressure, and reactor operation. Returning to the initial aims, the following can be concluded:

- The parallel difference test has been utilised to probe both steady and non-steady state behaviour of a model $Cu/ZnO/Al_2O_3$ catalyst. Under steady state conditions, this enabled integral response data to be segmented permitting more extensive data inputs to kinetic models. Critically, this allowed the relative equilibrium positions for methanol synthesis and water gas shift reactions to be tracked enabling inference on which directions of the reaction should be considered. The splitting of the steady state dataset into two parts based on water gas shift direction added an extra level of model discrimination to the analysis.
- A focus was placed on testing the model $Cu/ZnO/Al_2O_3$ catalyst under P_{CO}/P_{CO2} ratios between 1 and 10. Previous literature has demonstrated that significant changes to apparent methanol synthesis rate are seen under this range. A steady state kinetic model was developed based on the micro kinetic description of Vanden Bussche and Froment [14] and was able to capture the key adsorption constants and reactions under these conditions. The significant adsorption constants varied somewhat to the original model, particularly around the inclusion of surface carbonates. A key point here is that dominant surface populations in methanol synthesis can change as a function of the experimental space of conditions applied. Hence the conclusion from this work is to always begin a steady state modelling investigation with a wider spectrum of parameters from a micro kinetic model, before reducing to the key terms when estimating within the experimental space. The same is true when considering the kinetic description of back reactions such as FWGS. The second conclusion from this aim is that estimating kinetics on either side of a thermodynamic equilibrium position is a useful strategy to discriminate and probe kinetics models in these types of system.
- The model $Cu/ZnO/Al_2O_3$ catalyst was tested under dynamic start-up conditions where $CO/CO_2/H_2$ was introduced onto the freshly reduced material. The analysis of molar balance of carbon and oxygen species has provided insight into the development of methanol synthesis and reverse water gas shift (RWGS) activity over these types of catalyst. RWGS is seen to take place from the start, as CO_2 dissociates to CO and O.s on the catalyst surface. This allows for the development of a surface containing both O.s and s sites which is a basis for methanol synthesis activity, via bidentate CO_2 adsorption to form carbonates, over copper. Findings are consistent with the steady state kinetic model.
- Binary (Cu/ZnO and Cu/Al_2O_3) catalysts were also tested and modelled to assess which kinetic parameters are influenced by formulation. Methanol synthesis rate constant (k_1) was correlated with productivity and copper surface area, but in a

non-linear manner. Meanwhile, the RWGS rate constant, k_2, was almost constant between the binary and ternary catalysts suggesting no relationship between copper surface area and support choice, agreeing with previous literature. Further kinetic analysis of these materials would be useful, as the results show the redox balance of O.s and s sites is important in all three catalysts and tenuously, carbonate population decreases rapidly as a function of methanol synthesis activity and therefore copper surface area.

Future work in this area should extend to the investigation of CO/H_2 feeds. Under these conditions, a dramatic decrease in CH_3OH productivity is witnessed in comparison with low but not zero CO_2 feeds. Previous attempts to build steady state kinetic models under these conditions have encountered a number of issues, particularly relating to irreversible changes to catalyst activity as a function of conditions. The use of spatially discretised testing methods under both steady and non-steady state operation could be highly effective in elucidating changes to the catalyst and allow for a stronger comparison with the $CO/CO_2/H_2$ conditions explored in this paper. Again, the use of binary formulation will allow the relationship between catalyst components and functionality to be pinpointed.

Acknowledgements

SKW was supported by an Engineering Doctorate Studentship in Formulation Engineering at the University of Birmingham sponsored by the EPSRC (EP/G036713/1) and Johnson Matthey. The authors would also like to thank Colin Ranson, Rob Fletcher and Deborah Dodds (JM) for their help in this project.

Appendix A. Supplementary material

Supplementary data associated with this article can be found, in the online version, at http://dx.doi.org/10.1016/j.jcat.2016.01.025.

References

[1] D.B. Rasmussen, T.V.W. Janssens, B. Temel, T. Bligaard, B. Hinnemann, S. Helveg, J. Sehested, J. Catal. 293 (2012) 205–214.
[2] M.V. Twigg, Catalyst Handbook, second ed., Wolfe Publishing Ltd., 1989 (Chapter 9).
[3] V.E. Leonov, M.M. Karavaev, E.N. Tsybina, G.S. Petrischeva, Kinet. Katal. 14 (1973) 848.
[4] S.P.S. Andrew, at '7th Int. Con. of Catalysis'., Osaka, Japan, 7th July 1980.
[5] K. Klier, V. Chatikavanu, R.G. Herman, G.W. Simmons, J. Catal. 74 (1982) 343–360.
[6] G. Liu, D. Willcox, M. Garland, H.H. Kung, J. Catal. 96 (1985) 251–260.
[7] G.C. Chinchen, K.C. Waugh, D.A. Whan, Appl. Catal. 25 (1986) 101–107.
[8] M. Sahibzada, I.S. Metcalfe, D. Chadwick, J. Catal. 174 (1998) 111–118.
[9] V.P. Mochalin, G.I. Lin, A.Y. Rozovskii, Khim. Promst. 1 (1984) 11.
[10] T. Kubota, I. Hayakawa, H. Mabuse, K. Mori, K. Ushikoshi, T. Watanabe, M. Saito, Appl. Organometal. Chem. 15 (2001) 121–126.
[11] A.Y. Rosovskii, G.I. Lin, Top Catal. 22 (3–4) (2003) 137–150.
[12] G.H. Graaf, E.J. Stamhuis, A.A.C.M. Beenackers, Chem. Eng. Sci. 43 (12) (1988) 3185–3195.
[13] H.W. Lim, M. Park, S. Kang, H. Chae, J.W. Bae, K. Jun, Ind. Eng. Chem. Res. 48 (23) (2009) 10448–10455.
[14] K.M. Vanden Bussche, G.F. Froment, J. Catal. 161 (1996) 1–10.
[15] G.E. Parris, K. Klier, J. Catal. 97 (1986) 374–384.
[16] C.V. Ovesen, B.S. Clausen, J. Schiøtz, P. Stoltze, H. Topsøe, J.K. Nørskov, J. Catal. 168 (1997) 133–143.
[17] C.V. Ovesen, P. Stoltze, J.K. Nørskov, C.T. Campbell, J. Catal. 134 (1992) 445–468.
[18] K.C. Waugh, Catal. Today 53 (1999) 161–176.
[19] J. Nakamura, J.M. Campbell, C.T. Campbell, J. Chem. Soc. Faraday Trans. 86 (1990) 2725–2734.
[20] A. Coteron, A.N. Hayhurst, Chem. Eng. Sci. 49 (2) (1994) 209–221.
[21] M. Bowker, R.A. Hadden, R.A. Houghton, J.N.K. Hyland, K.C. Waugh, J. Catal. 109 (1988) 263–273.
[22] K.M. Vanden Bussche, G.F. Froment, Appl. Catal. A: Gen. 112 (1994) 37–55.
[23] G.C. Chinchen, M.S. Spencer, Catal. Today 10 (1991) 293–301.
[24] M. Peter, M.B. Fichtl, H. Ruland, S. Kaluza, M. Muhler, O. Hinrichsen, Chem. Eng. J. 203 (2012) 480–491.
[25] T.S. Askgaard, J.K. Norskov, C.V. Oversen, P. Stoltze, J. Catal. 156 (1995) 229–242.
[26] G.C. Chinchen, C.M. Hay, H.D. Vandervell, K.C. Waugh, J. Catal. 103 (1987) 79–86.
[27] K. Narita, N. Takeyawa, J. Kobayashi, I. Toyoshima, React. Kinet. Catal. Lett. 19 (1982) 91.
[28] C.F. Chu, K.M. Ng, AIChE J. 35 (1989) 148.
[29] S. Ergun, Chem. Eng. Prog. 49 (1952) 89–94.
[30] J. Perez-Ramirez, R.J. Berger, G. Mul, F. Kapteijn, J.A. Moulijn, Catal. Today 60 (2000) 93–109.
[31] H.H. Kung, Catal. Today 11 (1992) 443–453.
[32] L. Hanken, Master's Thesis, Norwegian University of Science and Technology, 1995.
[33] I. Løvik, M. Rønnekleiv, O. Olsvik, T. Hertzberg, Eur. Sym. on Comp. Aided Process Engineering, vol. 11, 2001, pp. 219–224.
[34] M.B. Fichtl, D. Schlereth, N. Jacobsen, I. Kasatkin, J. Schumann, M. Behrens, R. Schlögl, O. Hinrichsen, Appl. Catal. A: Gen. 502 (2015) 262–270.
[35] J.J. Birtill, Catal. Today 81 (2003) 531–545.
[36] S.K. Wilkinson, M.J.H. Simmons, E.H. Stitt, X. Baucherel, M.J. Watson, J. Catal. 299 (2013) 249–260.
[37] W.E. Stewart, M. Caracotsios, Computer-aided Modelling of Reactive Systems, John Wiley and Sons, 2008.
[38] M. Caracotsios, W.A.E. Stewart, Comp. Chem. Eng. 9 (4) (1985) 359–365.
[39] G.H. Graaf, P.J.J.M. Sijtsema, E.J. Stamhuis, G.E.H. Joosten, Chem. Eng. Sci. 41 (11) (1986) 2883–2890.
[40] G. Soave, Chem. Eng. Sci. 27 (1972) 1197–1203.
[41] J.C.J. Bart, R.P.A. Sneeden, Catal. Today 2 (1987) 1–124.
[42] P.B. Himelfarb, G.W. Simmons, K. Klier, R.G. Herman, J. Catal. 93 (1985) 442.
[43] P. Villa, P. Forzatti, G. Buzzi-Ferraris, G. Garone, I. Pasquon, Ind. Eng. Chem. Proc. Des. Dev. 24 (1985) 12–19.
[44] S.K. Wilkinson, I. McManus, H. Daly, J.M. Thompson, C. Hardacre, N. Sedaie Bonab, J. ten Dam, M.J.H. Simmons, C. D'Agostino, J. McGregor, L.F. Gladden, E. H. Stitt, J. Catal. 330 (2015) 362–373.